Permeability and Rigidity of Green River Shale Before and After Exposure to Water

Levent Taylan Ozgur Yildirim[1,2]
Department of Energy and Mineral Engineering;
EMS Energy Institute and G3 Center,
The Pennsylvania State University,
University Park, PA 16802
e-mail: lyildirim@tp.gov.tr

Derek Elsworth
Department of Energy and Mineral Engineering;
EMS Energy Institute and G3 Center;
Department of Geosciences,
The Pennsylvania State University,
University Park, PA 16802
e-mail: elsworth@psu.edu

John Yilin Wang
Department of Energy and Mineral Engineering;
EMS Energy Institute and G3 Center,
The Pennsylvania State University,
University Park, PA 16802
e-mail: john.wang@psu.edu

Acoustic travel times through Green River shale samples both parallel and perpendicular to bedding are measured to investigate water interactions with Green River shale and the impact of pertinent factors including exposure durations, pore pressure, effective stress, and anisotropy. To assist these analyses, X-ray diffraction (XRD) and permeability are also measured. Understanding petrophysical and rock properties before and after exposure to water is essential to optimize stimulation design in shale reservoirs. The XRD shows that the samples are clay-poor and mainly consist of carbonate minerals. Bedding-parallel and bedding-perpendicular permeability to non-sorbing He are measured before exposure to tap water to analyze permeability evolution under different stress conditions using the pressure transient method. The samples record very low permeabilities at recreated confining stresses, indicating that the shale requires stimulation. The permeability decreases as confining stress increases, while the permeability increases with increasing pore pressure. Acoustic travel time measurements show that compressional and shear wave velocities, and elastic moduli of the samples increase as confining stress increases before samples are exposed to tap water. This results in more rigid samples which exhibit higher fracture conductivity. The samples are saturated with tap water in containers at atmospheric pressure after the initial acoustic travel time measurements. Further acoustic travel time measurements and chemical elemental analysis in tap water show that quartz dissolves from the pore structure of the Green River shale, reducing the acoustic velocities, and elastic moduli of the samples that then exhibit lower rigidity and fracture conductivity.
[DOI: 10.1115/1.4056032]

Keywords: oil/gas reservoirs, petroleum engineering, unconventional petroleum

Introduction

From a petrophysical point of view, shale gas reservoirs mainly consist of clay- to silt-sized inorganic matrix and kerogen [1,2]. Shale gas reservoirs have low porosity and permeability and complex pore network. Horizontal drilling and multi-stage fracture treatments enabled the economic development of shale oil and gas resources. Both field and laboratory investigations are necessary to evaluate the petrophysical properties of surface and subsurface shale samples. The laboratory evaluation of shale is a prerequisite to improve stimulation design and operations [3]. The mineral assemblage is quantified using X-ray diffraction analysis [3,4]. The pressure transient method is used to determine the permeability [5,6]. The acoustic travel times of shale are measured to evaluate geomechanical properties [2,3].

The Eocene Green River shale was deposited in a fresh-water lake environment, and its overall thickness extends up to 3609 ft [7]. From bottom to top, it is subdivided into Tipton Shale, Wilkins Peak, and Laney Shale members [8]. It consists of dolomitic oil shales interbedded with carbonate-rich marginal lacustrine mudstones with oolitic limestones [7]. It is one of the major tight oil deposits. Recently, companies have been working on experimental field projects for oil shale recovery [9]. The estimated resources of Green River oil shale deposits have increased throughout the history of their development and are between 1.5 and 2.5 million barrels per acre [10].

The permeability and acoustic travel time measurements of the shale formations, including the Green River shale, were discussed in the literature. The permeability of commercial unconventional shale formations is less than 0.1 md [11]. Li et al. [12] discussed the evolution of permeability with effective stress in propped fractures using CH_4, N_2, CO_2, and He in the Green River shale. They stated that the permeability of shales, ranging from 10^{-3} to 10^{-7} md, is affected by different gas permeants. Moreover, the ultrasonic measurements of hydrocarbon source rocks and their anisotropy were previously studied [13,14]. The acoustic wave velocities of the Green River shale were also discussed [15–17]. The effects of geomechanical properties, i.e., Young's modulus, on the fracture conductivity of shales were studied [18]. A positive correlation between Young's modulus and fracture conductivity of shales was reported [18]. However, the response of petrophysical and rock properties of the Green River shale to exposure to stimulation fluids is not yet fully understood.

This paper is to further evaluate Green River shale outcrop samples using the following investigations: (1) X-ray diffraction analysis for qualitative and semi-quantitative mineralogy observations, (2) permeability measurements under different stress conditions using non-sorbing He (assumed to be an ideal gas) before exposure to tap water, and (3) acoustic compressional and shear wave travel time measurements under different confining stresses both before and after exposure to tap water. These define velocity anisotropy and changes in the geomechanical properties of Green River shale under different stress conditions, bedding plane orientations, and exposure times to tap water. These techniques and analyses could be used to evaluate other shale formations.

Experimental Methods

Materials and Sample Preparation. Four fine-grained outcrop samples of Green River shale are cored; two are parallel (#1 & #3) and two are perpendicular (#2 and #4) to the bedding plane. The samples are drilled from a Green River shale cube to obtain

[1]Corresponding author.
[2]Present Address: Turkish Petroleum Corporation, 06530 Ankara, Turkey.
Contributed by the Advanced Energy Systems Division of ASME for publication in the Journal of Energy Resources Technology. Manuscript received June 28, 2022; final manuscript received October 11, 2022; published online November 7, 2022. Assoc. Editor: Yan Jin.

Fig. 1 Green River shale block and samples drilled parallel and perpendicular to the bedding plane

Table 1 Length, mass, and bulk density of core plug samples used in this study

Physical property	Sample #1	Sample #2	Sample #3	Sample #4
Length (ft)	0.17000	0.16000	0.17000	0.15000
Diameter (ft)	0.08000	0.08000	0.08000	0.08000
Mass (lb)	0.12928	0.12621	0.13457	0.11903
Bulk density (lb/ft^3)	141.020	141.020	141.580	142.430

cylindrical-shaped core plugs as shown in Fig. 1. The physical dimensions of the core plugs used for experiments in this study are shown in Table 1.

X-Ray Diffraction Analysis. The mineral composition of fine powders of Green River shale is identified by X-ray diffraction. A PANalytical Empyrean diffractometer equipped with Cu K-alpha radiation is used to collect the data. Qualitative phase identification and semi-quantitative compositional analysis are performed using Jade 2010 software (Materials Data Inc., Livermore, CA). Both qualitative phase identification and semi-quantitative compositional analysis utilized reference files from the International Center for Diffraction Data (ICDD). Whole pattern fitting analysis is used for semi-quantitative mineralogical analysis.

Permeability Evolution. Permeability measurements are conducted for 2 Green River shale samples (#3 and #4). Samples #3 and #4 are cored parallel and perpendicular to bedding to examine the permeability evolution of Green River shale to non-sorbing He gas as confining stresses and pore pressures change at room temperature. The experimental measurements are performed using the pressure transient method under dry conditions before the samples are exposed to tap water.

The experimental apparatus used for permeability measurements is a triaxial core holder as shown in Fig. 2. The triaxial core holder enables experiments on cylindrical samples of 1 in. in diameter and up to 4 in. in length. The experimental setup allows the application of uniform confining stresses up to 5076 psi using dual-cylinder syringe pump in radial and axial directions using water, and pore fluid pressure up to 2465 psi using another dual-cylinder syringe pump through upstream and downstream reservoirs. A pore fluid tank can be used for the case where extra pore fluid must be injected into the pump. Pressure transducers on the upstream and downstream reservoirs monitor the pore fluid pressures [19].

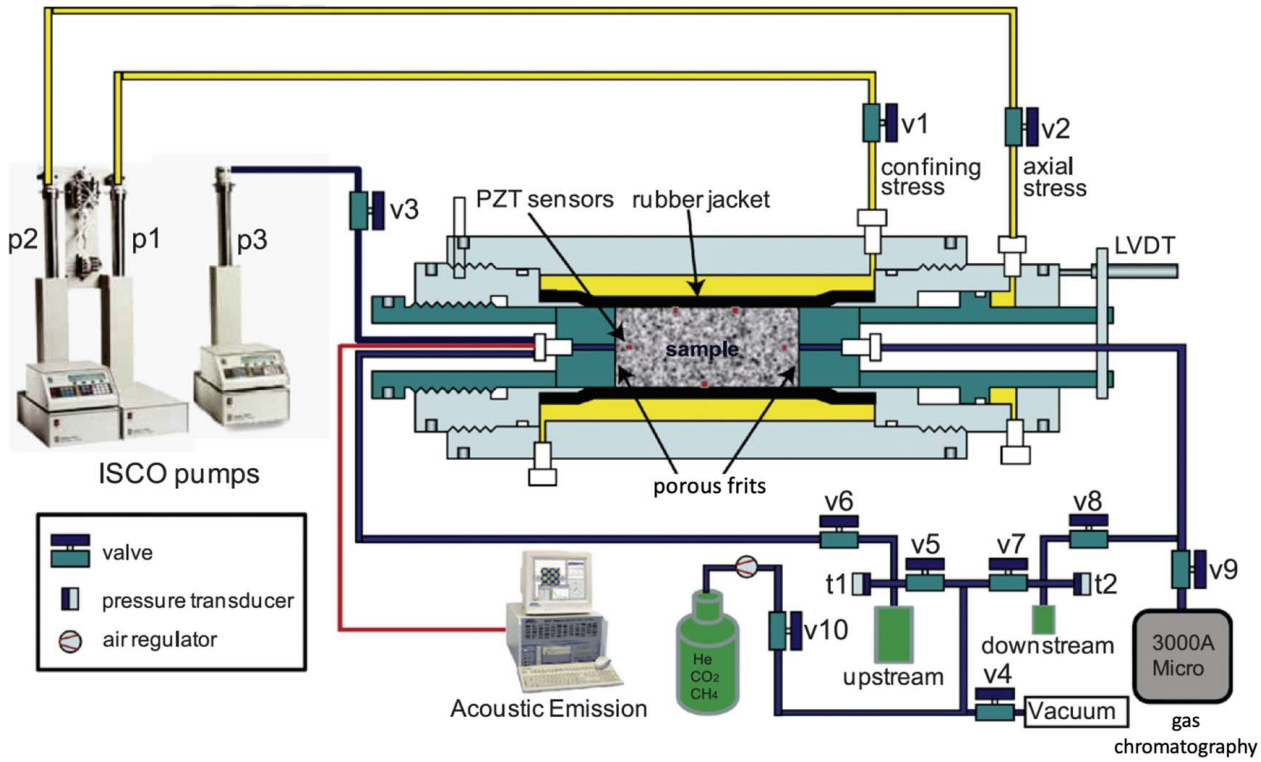

Fig. 2 Triaxial transient pulse test permeability measurement setup at G3 center at Penn State University [19]

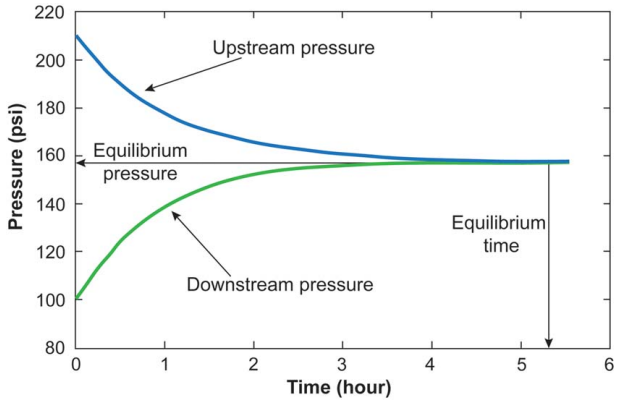

Fig. 3 Equilibrium process in the pressure transient method

The cylindrical sample is placed between two cylindrical steel endcaps (1 in. in diameter and 1 in. long). The endcaps are plumbed with flowlines with the fluid flow distributed across the end of the sample at the endcap-to-sample interface by a porous frit. This ensures that the upstream and downstream pressures are uniformly distributed across the sample and that the principal resistance to flow is in the sample, not the frit. The endcaps contain piezoelectric (PZT) transducers in transmission and receiver modes. The sample, sandwiched between the frits and encaps, is installed within a polyvinyl chloride (PVC) rubber jacket into the core holder. The function of the rubber jacket is to isolate the materials inside it from the confining fluid. Pressure, flowrate, and fluid volume signals obtained from the ISCO pumps are recorded using (National Instruments) LabVIEW program via a serial connection (RS-232) between the pumps and the logging computer. Output signals from a single linear variable differential transformer (LVDT) and two pressure transducers are converted at 16-bit resolution using a 16-channel data acquisition system (National Instruments—USB 6211). The signals are then logged digitally at a sampling rate from 1 Hz to 1 kHz by a computer using LabVIEW [19].

The samples are placed in an oven under 40 °C under vacuum for 24 h before they are installed into the core holder. The system is also vacuum desaturated to evacuate air from the system. The pressure transient method is used to measure the permeability of the Green River shale samples. In the pressure transient method, pore fluid is injected from the upstream reservoirs at incremented pressure levels. The pressure of the upstream reservoir is higher than that of the downstream so that the pore fluid flows from upstream to downstream through the core sample.

As the pore fluid flows from the upstream to the downstream reservoir through the sample, the pressure of the upstream reservoir decreases and that of the downstream reservoir increases, ultimately equilibrating as shown in Fig. 3. The time to reach equilibrium pressure is a measure of permeability. The non-sorbing He gas is used as the pore fluid in the permeability experiments. The volume of He is kept low by assembling downstream and upstream reservoirs at low volumes since the permeability of shale is low. The volumes of the upstream and downstream reservoir are 0.503 cm^3 and 0.600 cm^3, respectively. In the pressure transient method, there is a relatively small pressure difference between upstream and downstream reservoirs when compared to the steady-state method (downstream reservoir is open to the atmosphere). The pressure transient method would provide conditions closer to the in-situ condition than the steady-state method.

The experimental and analytical details of the pressure transient method for determining permeability can be found in Refs. [5,6]. The governing equation for the pressure pulse through the core sample can be written as follows in Eqs. (1) and (2) as previously discussed [5,6]:

$$P_u(t) - P_d(t) = (P_u(t_0) - P_d(t_0))^{e^{-\alpha t}} \tag{1}$$

$$k = \frac{\alpha \mu c L V_u V_d}{A(V_u + V_d)} \tag{2}$$

where $P_u(t) - P_d(t)$ is the pressure difference between the upstream and downstream reservoirs at time t. $P_u(t_0) - P_d(t_0)$ is the initial pressure difference between upstream and downstream reservoirs at time t_0. α is the slope of the line when plotting the pressure decay $P_u(t) - P_d(t)$ on semi-log paper against time. k is the permeability of the sample. A and L are the cross-sectional area and length of the sample. μ and c are the dynamic viscosity and compressibility of the gas. V_u and V_d are the volumes of the upstream and downstream reservoirs. The compressibility is taken as $1/P_{eq}$ since the gas is assumed to be ideal. P_{eq} is the final equilibrium pressure in the system when the pressures of the upstream and downstream reservoirs converge at the conclusion of the test.

Permeability experiments on Green River shale both parallel and perpendicular to bedding are conducted under confining stresses of 870 psi, 1740 psi, and 2610 psi at a constant pore pressure of 461 psi and with pore pressures of 170 psi, 461 psi, and 605 psi under a constant confining stress of 870 psi to observe how permeability changes as confining stresses and pore pressures increase. First, a pressure increment is applied from the confining fluid pump into the vessel to apply confining stress. Then, the pore fluid pump is used to inject He gas into the upstream and downstream reservoirs at desired pressure levels. Finally, valves

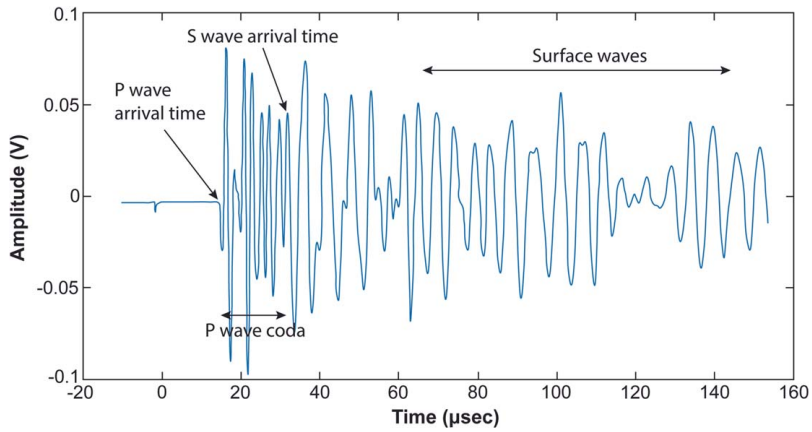

Fig. 4 Amplitude (V) versus time (μsec) plot for sample #4 perpendicular to bedding plane under 2610 psi confining stress

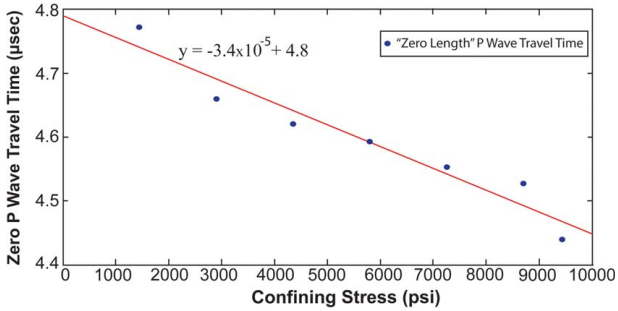

Fig. 5 "Zero Length" P wave travel time through the end caps and porous frits (μsec) versus confining stress (psi)

connecting the reservoirs and the vessel are opened to allow gas flow from upstream to downstream reservoirs through the sample. Higher upstream pressure is assigned so that the direction of flow is from upstream to downstream through the triaxial core holder.

Acoustic Travel Time Measurements. We measure acoustic travel time to evaluate original geomechanical properties and their evolution under various confining stresses and with different water interaction times after the permeability experiments under dry conditions are completed. Four samples of the Green River shale are used in the experiments. First, the experiments are conducted before exposure to tap water. After the initial experiments, samples are saturated with tap water in containers at atmospheric pressure to observe ionic exchange and dissolution between the Green River shale and the tap water at different times and along bedding planes. The acoustic travel times are measured for samples #1, #2, and #4 after they are saturated for 35 days. The acoustic travel times are measured for sample #3 after it is saturated for ~120 days. The samples are oven dried between the acoustic travel time measurements. The aim of conducting the experiments both before and then after exposure to tap water is to observe velocity anisotropy and changes in geomechanical properties and evaluate rigidity and fracture conductivity of the analyzed samples.

The experimental apparatus used for acoustic travel time measurements is the same triaxial core holder but with an ultrasonic pulser–receiver as shown in Fig. 2. The triaxial core holder allows experiments on cylindrical samples 1 inch in diameter and up to 2.3 in. in length. Confining stresses up to 9427 psi can be applied using Teledyne ISCO d-series pump in radial and axial directions. Pressure transducers are installed within Global Digital Systems (GDS) pumps on the upstream and downstream reservoirs and pore fluid pressure can be adjusted using the pumps. Distilled water is used as pore fluid within the pumps.

The cylindrical sample is held between two metal porous frits and two end caps within an impermeable membrane. An Olympus Panametrics Model 5058PR ultrasonic pulser–receiver is attached to the triaxial core holder at each end using tubes of distribution end caps with PZT sensors to send sound waves through the sample after confining stresses are assigned. The function of the ultrasonic pulser–receiver is to measure the energy of acoustic waves at various sampling rates. The sampling rate and number of records to stacks during the transmission, as well as the P- and S-wave arrival times, are controlled using LabVIEW software panel located on top of the ultrasonic pulser–receiver.

Compressional and shear wave travel time measurements on Green River shale samples both parallel and perpendicular to bedding plane are conducted under three confining stresses at a constant pore fluid pressure before and after exposure to tap water. The system is vacuum desaturated to evacuate air from the system before experiments.

The ultrasonic pulse transmission method is applied to measure the acoustic travel times. When the samples are stressed to the assigned confining stress, the pulser–receiver is attached to the core holder and velocities are measured at 25 and 50 MHz sampling rates for experiments before and after exposure to tap water, respectively. The samples are stacked 100 times resulting in 100 waveforms as the sound waves are transmitted within the sample 100 times. Amplitudes are recorded by the pulser–receiver.

P wave arrival time is picked at the first deflection in the energy of waves. Since P waves travel faster than S waves, S-wave arrival time is greater than P wave arrival time. Continuous high-frequency P waves representing P wave coda interfere with S waves and makes it challenging to accurately pick the first S-wave arrival time. The first S-wave arrival time is picked at a relatively larger amplitude and lower frequency coming after the P wave coda (Fig. 4).

The ultrasonic pulser–receiver transmits acoustic waves along the sample and between the PZT sensors in the opposing endcaps, including the intervening (two) metal porous frits, and a fraction of the length of the two endcaps. The length of the two porous frits and two end caps are 1 in. in total. The diameter of the porous frits is 1 in. The travel times through the porous frits and end caps ("zero length" travel times) are subtracted from picked (total) travel times for the travel time correction.

The "zero length" P wave travel times are obtained by conducting pulse transmission experiments on two endcaps and two porous frits under various confining stresses. The "zero length" P wave travel times are calculated under 870, 1740, and 2610 psi confining stresses using the expression of the linear relation between "zero

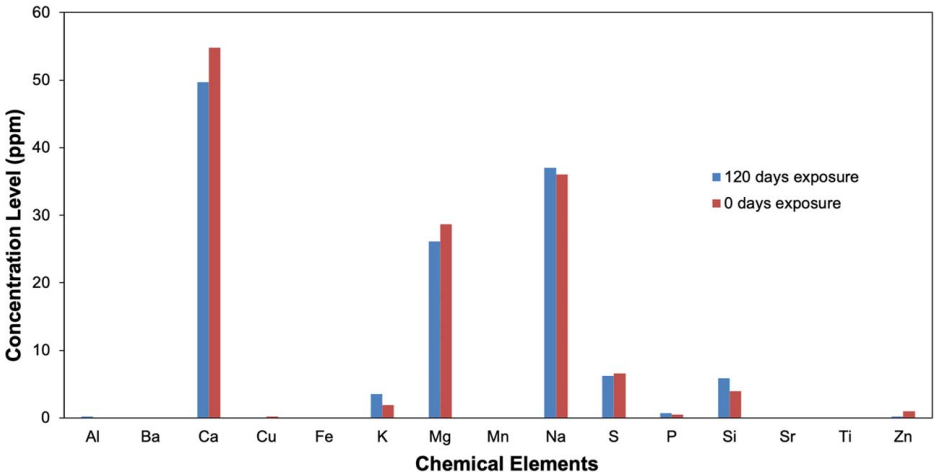

Fig. 6 Change of concentration level of chemical elements in tap water used to saturate sample #3 after 120 days of interaction

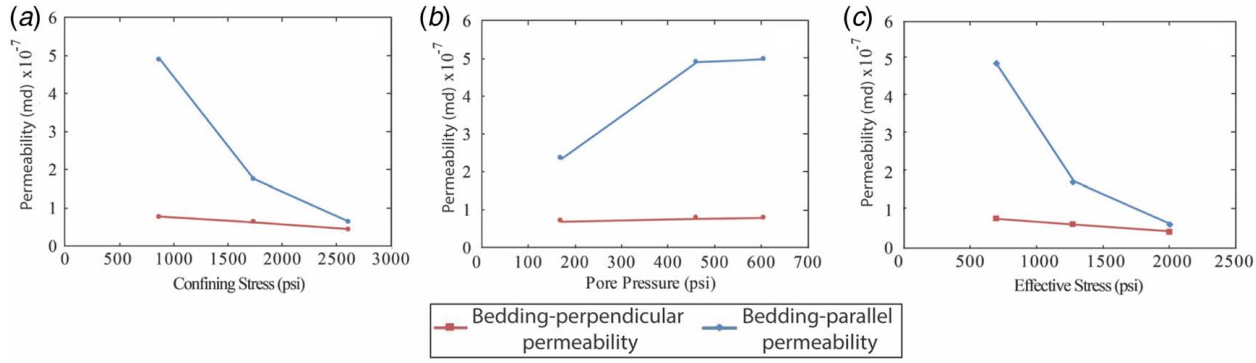

Fig. 7 Bedding-parallel and bedding-perpendicular permeability evolution of Green River shale as functions of (*a*) confining stress, (*b*) pore pressure, and (*c*) effective stress

Table 2 Compressional and shear wave travel time and velocity results of experiments before exposure to tap water under various confining stresses

Sample	Confining stress (psi)	t_c (μs)	t_S (μs)	v_c (ft/s)	v_S (ft/s)
#1 Parallel	870.2	11.52	24.89	14,756.94	6830.05
	1740.5	11.43	24.82	14,873.14	6849.32
	2610.7	11.30	24.72	15,044.25	6877.02
#2 Perpendicular	870.2	12.40	25.33	12,903.23	6316.62
	1740.5	11.99	25.26	13,344.45	6334.13
	2610.7	11.90	25.16	13,445.38	6359.30
#3 Parallel	870.2	12.32	26.29	13,798.70	6466.34
	1740.5	12.15	26.14	13,991.77	6503.44
	2610.7	12.10	26.08	14,049.59	6518.40
#4 Perpendicular	870.2	11.64	25.05	12,886.60	5988.02
	1740.5	11.47	24.98	13,077.59	6004.80
	2610.7	11.42	24.96	13,134.85	6009.62

length" P wave travel time versus confining stress (Fig. 5). The "zero length" S-wave travel times at the corresponding confining stresses are calculated by taking the Poisson ratio of stainless-steel end cap and porous frits as 0.29 as stated in Ref. [20]. The "zero length" S-wave travel time can be calculated by multiplying the compressional to shear slowness ratio and "zero length" P wave travel time.

After the "zero length" P wave and S-wave travel times are calculated, the corrected travel time of the samples is calculated by subtracting the "zero length" travel times from picked (total) travel times. Compressional and shear velocities are calculated by dividing the length of the core plug sample into corrected travel times while the measurements are being conducted.

The change of concentration of chemical elements in tap water used to saturate samples after ~120 days of interaction obtained by Inductively Coupled Plasma Atomic Emission Spectrometry is shown in Fig. 6. Ionic exchange between water and minerals in samples results in an increase in Si concentration and a decrease in Ca and Mg concentration.

Results

We examine the mineral content, evolution of bedding-parallel and bedding-perpendicular permeability, seismic velocity, anisotropy, and geomechanical properties of the Green River shale.

Table 3 Compressional and shear wave travel time and velocity results of experiments after exposure to tap water under various confining stresses

Sample-exposure time	Confining stress (psi)	t_c (μs)	t_S (μs)	v_c (ft/s	v_S (ft/s)
#1	870.2	11.62	24.91	14,629.95	6824.57
35 Days	1740.5	11.53	24.54	14,744.15	6841.05
	2610.7	11.36	24.36	14,964.79	6865.91
#2	870.2	12.90	25.45	12,403.10	6286.84
35 Days	1740.5	12.63	25.36	12,668.25	6309.15
	2610.7	12.42	25.26	12,882.45	6334.13
#3	870.2	12.86	25.87	13,219.28	6456.51
120 Days	1740.5	12.65	25.78	13,438.74	6488.55
	2610.7	12.46	25.70	13,643.66	6508.42
#4	870.2	11.68	24.83	12,842.47	5976.10
35 Days	1740.5	11.49	24.70	13,054.83	5997.60
	2610.7	11.32	24.62	13,250.88	6004.80

Table 4 Algebraic expressions for geomechanical properties [21]

Geomechanical Property	Algebraic Expression	
Compressional to shear slowness ratio	$\frac{v_c}{v_s}$	(3)
Poisson's ratio	$\frac{0.5 \times R_v^2 - 1}{R_v^2 - 1}$	(4)
Shear modulus, psi	$2.1584 \times 10^{-4} \rho_b v_s^2$	(5)
Young's modulus, psi	$2G(1 + v)$	(6)
Bulk modulus, psi	$2.1584 \times 10^{-4} \rho_b \left(v_c^2 - \frac{4}{3} v_s^2 \right)$	(7)

X-Ray Diffraction Analysis. Phase identification and whole pattern fitting semi-quantitative analysis of the diffraction patterns indicate that the mineralogy of the Green River shale is dominantly dolomite and calcium carbonate with average composition: 36.3% dolomite, 21.2% calcite, 12.5% analcime, 10.7% albite, 10.4% quartz, and 9.0% orthoclase mineral. The Green River shale is generally composed of light gray, calcareous, dolomitic mudstones, shales, marls, and claystones [8]. The analcime could be derived from the alteration of smectite. The presence of orthoclase indicates that the source material of the analyzed samples could be volcanic ash [8]. The analyzed sample belongs to carbonate-rich and clay-poor intervals of Wilkins Peak member or Laney Shale member [8] of the Green River shale.

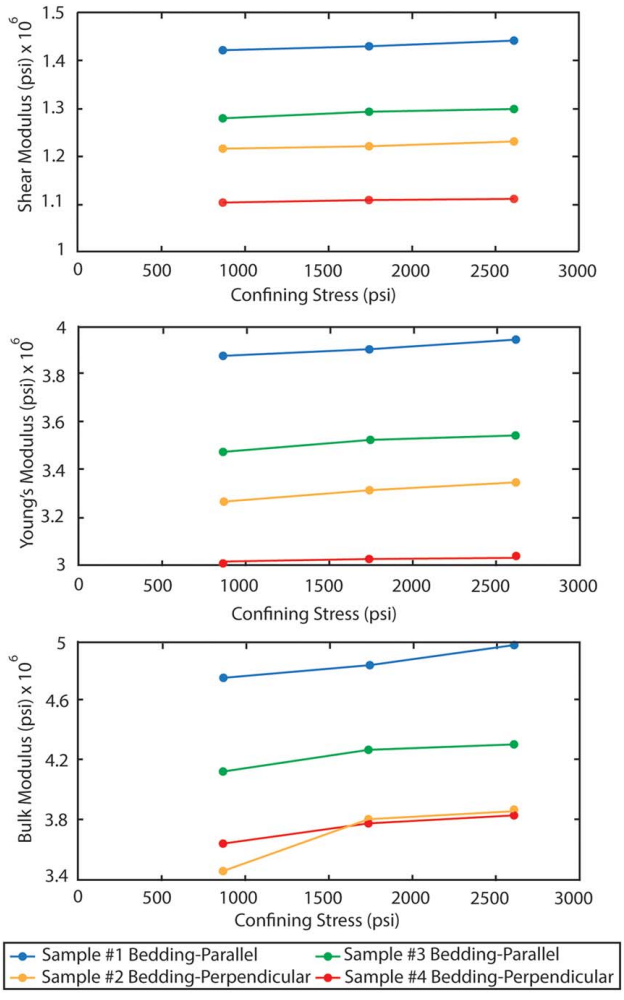

Fig. 8 Geomechanical properties versus confining stress before exposure to water for Green River Shale

Permeability Evolution. The permeability of the Green River shale samples measured both parallel and perpendicular to bedding under various confining stresses and pore pressures are calculated. Permeability of Green River shale is in the order of 10^{-7} millidarcy parallel to bedding and 10^{-8} millidarcy perpendicular to bedding. Bedding-parallel and bedding-perpendicular permeability evolution of Green River shale as functions of confining stress, pore pressure, and effective stress is shown in Fig. 7. Effective stress is the difference between confining stress and pore pressure inside the sample as previously studied [19].

Acoustic Travel Time Measurements. Compressional and shear wave travel times under various confining stresses are calculated after compressional and shear wave arrivals are picked (Fig. 4). The results for compressional and shear wave travel times under various confining stresses of initial measurements are listed in Table 2. The compressional wave travel times range from 12,903.23 ft/s to 15,044.25 ft/s under various confining stresses before exposure to water.

The acoustic travel time measurements are initially conducted for the samples before they are exposed to tap water. Then, the acoustic travel time measurements are conducted after the samples are exposed to tap water. The samples are dried in an oven between the experiments to remove the tap water.

After the samples are exposed to tap water, compressional and shear wave travel times and velocities are calculated and shown in Table 3. The compressional wave travel times range from 12,403.10 ft/s to 14,964.79 ft/s under various confining stresses after exposure to water. Compressional and shear wave travel times decrease as confining stress increases. Shear, Young's, and bulk moduli of the samples are calculated based on these acoustic travel times from Eqs. (3)–(7) shown in Table 4 as previously discussed [21].

The shear modulus, Young's modulus, and bulk modulus under different confining stresses for Green River shale samples parallel and perpendicular to bedding before exposure to tap water are shown in Fig. 8. Shear modulus or resistance of Green River shale samples against shear stress increases as confining stress increases. Young's modulus or resistance of Green River shale samples against applied stress in one direction increases as confining stress increases. Bulk modulus or resistance of Green River shale samples against uniform compression increases as confining stress increases.

The change of shear modulus, Young's modulus, and bulk modulus as functions of exposure time with tap water in Green River shale samples parallel and perpendicular to bedding at 870 psi confining stress are shown in Fig. 9. After samples are exposed to tap water, compressional and shear wave travel times and velocities are calculated. Shear modulus slightly decreases during long-term exposure of Green River shale samples to tap water. Therefore, the resistance of Green River shale to shear stress slightly decreases as it is exposed to tap water. Young's modulus, the resistance of Green River shale to applied stress in one direction, decreases during long-term exposure of the samples to tap water. Bulk modulus, the resistance of Green River shale samples against uniform compression, slightly decreases during long-term exposure of the samples to tap water.

Discussion

The permeability of the analyzed Green River shale samples decreases with increasing confining stress (Fig. 7(*a*)), which agrees with previous observations [22]. Bedding-parallel permeability, the ability of flow of pore fluid parallel to bedding, shows

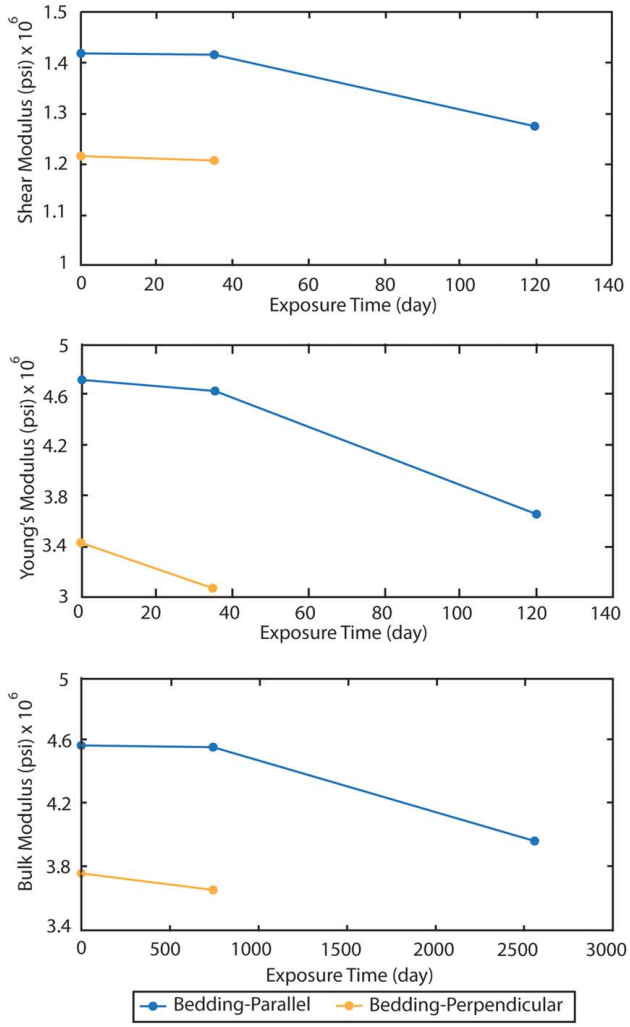

Fig. 9 Geomechanical properties versus exposure time after exposure to water for Green River Shale under 870 psi confining stress

a larger reduction from 4.89×10^{-7} md to 6.34×10^{-8} md as confining stress increases from 870 psi to 2610 psi. Conversely, bedding-perpendicular permeability, the ability of flow of pore fluid perpendicular to bedding, is less than bedding-parallel permeability and it decreases from 7.69×10^{-8} md to 4.33×10^{-8} md as confining stress increases from 870 psi to 2610 psi for non-sorbing He gas.

The permeability increases with increasing pore pressure for non-sorbing gas as previously discussed [12] (Fig. 7(*b*)). The bedding-parallel permeability shows a larger increase from 2.34×10^{-7} md to 4.98×10^{-7} md as pore pressure increases from 170 psi to 605 psi. Conversely, the bedding-perpendicular permeability, the ability for the flow of pore fluid perpendicular to bedding, is less than the bedding-parallel permeability and shows a slight increase from 6.91×10^{-8} md to 7.82×10^{-8} md as pore pressure increases from 170 psi to 605 psi. Zhou et al. [22] stated that matrix- and fracture permeabilities of shales decrease during the imbibition of fracture fluids since clay swelling reduces the permeability. However, the permeability of Green River shale in our measurements is not affected by the swelling of clay minerals since no clay mineral was observed in the analyzed samples. This contributes to an increase in permeability under various pore pressures.

Increased effective stress generally decreases bedding-perpendicular and bedding-parallel permeability of the analyzed Green River shale samples for the same gas permeant as previously studied [12,19,23–25]. The bedding-parallel permeability shows a larger reduction when compared to bedding-perpendicular permeability as effective stress increases (Fig. 7(*c*)).

The compressional wave velocities measured in the direction perpendicular to bedding for Green River shale range from 12,886.60 ft/s to 13,344.45 ft/s. Vernik and Nur [13] stated that extremely low compressional wave velocities, ranging from 9908 ft/sec to 13,222 ft/s, in the direction perpendicular to bedding imply strong velocity anisotropy for organic-rich Bakken shale when compared to organic-lean shales. The velocity difference between the direction perpendicular and parallel to bedding is much higher in organic-rich Bakken shale [13] than the Green River shale in our study. Therefore, the Green River shale in our study is not as strong as the organic-rich Bakken shale studied in Ref. [13] in terms of velocity anisotropy and can be characterized as organic-lean source rock based on relatively high compressional wave velocities in the direction perpendicular to bedding.

Compressional and shear wave velocities of Green River shale increase with increased confining stress as previously discussed [26]. Shear, Young's, and bulk moduli of the Green River shale before exposure to water increase as confining stress increases (Fig. 8), resulting in more rigid samples and a concomitant increase in fracture conductivity, as previously studied [18].

Compressional and shear wave velocities decrease as the Green River shale is exposed to tap water. Shear, Young's, and bulk moduli of the Green River shale decrease after exposure to tap water (Fig. 9). Dissolution of quartz from the pore structure could reduce moduli and acoustic velocities of the samples as confirmed by an increase in the concentration of Si element in tap water (Fig. 6). This implies a lower fracture conductivity of the analyzed samples, which agrees with previous observations [18].

Conclusions

We evaluate outcrop samples of Green River shale oriented both parallel and perpendicular to bedding through X-ray diffraction analysis, permeability measurements, and acoustic travel time experiments. X-ray diffraction is conducted to quantitatively determine the mineralogy of the Green River shale. Permeability measurements are conducted to observe permeability evolution under different confining stresses and pore pressures before stimulation treatments. Acoustic travel time measurements are conducted to observe changes in longitudinal and shear wave velocities and geomechanical properties under different confining stresses both before and after exposure to water. Therefore, this study attempts to apply state-of-the-art laboratory techniques and analyses to evaluate shale gas reservoirs, with a focus on petrophysical and rock properties both before and after exposure to water. Conclusions include the following:

- X-ray diffraction results confirm that the Green River shale is comprised of carbonate, analcime, albite, orthoclase, and quartz. The sample belongs to the carbonate-rich and clay-poor intervals of the Wilkins Peak member or Laney Shale member of the Green River shale.
- The permeability of the Green River shale samples increases as pore pressure increases from 170 psi to 605 psi. The permeability does not reduce since there is no swelling of clay minerals. The permeability of the Green River shale samples decreases as confining stress increases from 870 psi to 2610 psi. Bedding-parallel permeability is greater than bedding-perpendicular permeability by an order of magnitude. The bedding-parallel permeability is more sensitive to confining stress, pore pressure, and effective stress when compared to the bedding-perpendicular permeability. As permeability magnitudes are very low, further stimulation design, such as hydraulic fracturing for Green River shale, is necessary to increase the permeability using different fracturing fluids at different saturation levels and interaction times.
- Based on the relatively low difference in compressional wave velocities between the direction to perpendicular and parallel to bedding before exposure to tap water, the Green River shale is not as strong as organic-rich black shales in terms of

velocity anisotropy and can be characterized as organic-lean source rock.
- Acoustic travel time experiments show that compressional and shear wave velocities increase as confining stress increases. Green River shale tends to be more rigid and has higher shear, Young's, and bulk moduli.
- Conversely, compressional and shear wave velocities decrease during experiments following exposure to water. The framework minerals (i.e., quartz) are likely to be dissolved from the pore structure resulting in lower moduli and acoustic velocities of the Green River shale.

The new understanding and evaluation methods in this study could help improve stimulation design and operations in shale reservoirs.

Acknowledgment

The authors gratefully acknowledge the financial support of the Turkish Petroleum Corporation (TPAO), the National Petroleum Exploration and Production Company of Turkey. This study was presented at the 53rd U.S. Rock Mechanics/Geomechanics Symposium, June 2019.

Conflict of Interest

There are no conflicts of interest.

Data Availability Statement

The data sets generated and supporting the findings of this article are obtainable from the corresponding author upon reasonable request.

Nomenclature

c = compressibility of the gas, 1/psi
k = permeability, md
t = time taken for discharge between upstream and downstream reservoirs, s
v = Poisson's ratio
A = cross-sectional area, ft^2
E = Young's modulus, psi
G = shear modulus, psi
K = bulk modulus, psi
L = length of core plug sample, ft
t_c = compressional wave travel time, μs
t_s = shear wave travel time, μs
v_c = compressional wave velocity, ft/μs
v_s = shear wave velocity, ft/μs
P_{eq} = equilibrium pressure, psi
R_v = compressional to shear slowness ratio
V_d = volume of downstream reservoir, ft^3
V_u = volume of upstream reservoir, ft^3
$P_d(t)$ = downstream reservoir pressure at time t, psi
$P_d(t_0)$ = initial downstream reservoir pressure at time t_0, psi
$P_u(t)$ = upstream reservoir pressure at time t, psi
$P_u(t_0)$ = initial upstream reservoir pressure at time t_0, psi
α = slope of the line of pressure difference between the reservoirs, 1/s
μ = dynamic viscosity, cp
ρ_b = bulk density, lb/ft^3

References

[1] Potter, P. E., Maynard, J. B., and Depetris, P. J., 2005, *Mud and Mudstones*, Springer-Verlag, Berlin/Heidelberg.
[2] Glorioso, J. C., and Rattia, A., 2012, "Unconventional Reservoirs: Basic Petrophysical Concepts for Shale Gas," SPE/EAGE Unconventional Resources Conference and Exhibition Held in Vienna, Austria, Mar. 20–22, 2012, Paper No. SPE 153004.
[3] Sondergeld, C. H., Newsham, K. E., Comisky, J. T., Rice, M. C., and Rai, C. S., 2010, "Petrophysical Considerations in Evaluating and Producing Shale Gas Resources," Soc. Pet. Eng., pp. 1–34.
[4] Clennell, M. B., Dewhurst, D. N., and Raven, M., 2006, "Shale Petrophysics: Electrical, Dielectric and Nuclear Magnetic Resonance Studies of Shales and Clays," Proceedings of the 47th SPWLA Annual Logging Symposium, Veracruz, Mexico, June 4–7, pp. 1–34.
[5] Brace, W. F., Walsh, J. B., and Frangos, W. T., 1968, "Permeability of Granite Under High Pressure," J. Geophys. Res., **73**(6), pp. 2225–2236.
[6] Hsieh, P. A., Tracy, J. V., Neuzil, C. E., Bredehoeft, J. D., and Silliman, S. E., 1981, "A Transient Laboratory Method for Determining the Hydraulic Properties of 'Tight' Rocks-I Theory," Int. J. Rock Mech. Min. Sci. Geomech. Abstr., **18**(3), pp. 245–252.
[7] Self, J. G., Johnson, R. C., Brownfield, M. E., and Mercier, T. J., 2010, "Stratigraphic Cross Sections of the Eocene Green River Formation in the Piceance Basin, Northwestern Colorado," U.S. Geological Survey Digital Data Series, DDS-69-Y, Chaps. 5 and 7.
[8] Tank, R. W., 1972, "Clay minerals of the Green River Formation (Eocene) of Wyoming: Clay Minerals", v. 9, pp. 297-308.
[9] Dyni, J. R., 2006, "Geology and Resources of Some World Oil-Shale Deposits," U.S. Geological Survey Scientific Investigations Report, Report No. 2005-5294, p. 42.
[10] Williams, P., 2007, "Green River Oil Shale," E&P Momentum, **27**(7), p. 73.
[11] Tütüncü, A., 2019, "Conventional vs Unconventional Resources; Similarities and Differences," Lecture, Turkish Petroleum Corporation Headquarters, July 2–4, 2019, Ankara, Turkey.
[12] Li, X., Feng, Z., Han, G., and Elsworth, D., 2017, "Permeability Evolution of Propped Artificial Fractures in Green River Shale," Rock Mech. Rock. Eng., **50**(6), pp. 1473–1485.
[13] Vernik, L., and Nur, A., 1992, "Ultrasonic Velocity and Anisotropy of Hydrocarbon Source Rocks," Geophysics, v., **57**(5), pp. 727–735.
[14] Sondergeld, C. H., Chandra, S. R., Margesson, R. W., and Whidden, K., 2000, "Ultrasonic Measurement of Anisotropy on the Kimmeridge Shale," SEG Expand. Abst., **19**(1), pp. 1858–1861.
[15] Podio, A. L., Gregory, A. R., and Gray, K. R., 1968, "Dynamic Properties of Dry and Water Saturated Green River Shale Under Stress," Proceedings of the SPE 42nd Annual Fall Meeting, Houston, TX, Oct. 1967.
[16] Fang, Y., Elsworth, D., Wang, C., Ishibashi, T., and Fitts, J. P., 2017, "Frictional Stability-Permeability Relationships for Fractures in Shales," J. Geophys. Res. Solid Earth, **122**(3), pp. 1760–1776.
[17] Jia, Y. Z., Fang, Y., Elsworth, D., and Wu, W., 2020, "Slip Velocity Dependency of Friction-Permeability Response of Shale Fractures," Rock Mech. Rock. Eng., **53**(5), pp. 1–13.
[18] Kainer, C., Guerra, D., Zhu, D., and Hill, A. D., 2017, "A Comparative Analysis of Rock Properties and Fracture Conductivity in Shale Plays," SPE Hydraulic Fracturing Technology Conference, The Woodlands, TX, Jan. 24–26. Paper No. SPE-184877-MS.
[19] Wang, S., Elsworth, D., and Liu, J., 2012, "Permeability Evolution in Fractured Coal: The Roles of Fracture Geometry and Water-Content," Int. J. Coal Geol., **87**(2011), pp. 13–25.
[20] Dupen, B., 2016, *Applied Strength of Materials for Engineering Technology*, 10th ed., Manufacturing and Construction Engineering Technology, Faculty Publications, Purdue University. http://opus.ipfw.edu/mcetid_facpubs/48.
[21] Dewan, J. T., 1983, *Essentials of Modern Open Hole Log Interpretation*, PennWell Corporation, Tulsa, OK.
[22] Zhou, Z., Abass, H., Li, X., and Teklu, T., 2016, "Experimental Investigation of the Effect of Imbibition on Shale Permeability During Hydraulic Fracturing," J. Nat. Gas Sci. Eng., **2016**(29), pp. 413–430.
[23] Durucan, S., and Edwards, J. S., 1986, "The Effects of Stress and Fracturing on Permeability of Coal," Mining Sci. Technol., **3**(3), pp. 205–216.
[24] Somerton, W. H., Soylemezoglu, I. M., and Dudley, R. C., 1975, "Effect of Stress on Permeability of Coal," Int. J. Rock Mech. Mining Sci. Geomech. Abstr., **12**(5–6), pp. 129–145.
[25] Wu, Y., Liu, J., Elsworth, D., Chen, Z., Connell, L., and Pan, Z., 2010, "Dual Poroelastic Response of a Coal Seam to CO2 Injection," Int. J. Greenhouse Gas Control, **4**(4), pp. 668–678.
[26] Miller, P. K., 2015, "Experimental Investigation of Permeability and Mechanical Evolution of Cataclastic Deformation Bands," Dissertation, Geosciences Department of the Pennsylvania State University, State College, PA.